



1 **Measurement Report: Seasonal variation and**
2 **anthropogenic influence on cloud condensation nuclei**
3 **(CCN) activity in the South China Sea: Insights from**
4 **shipborne observations during summer and winter of**
5 **2021**

6 Hengjia Ou¹, Mingfu Cai², Yongyun Zhang¹, Xue Ni¹, Baoling Liang³, Qibin Sun^{4,5},

7 Shixin Mai¹, Cuizhi Sun⁶, Shengzhen Zhou¹, Haichao Wang¹, Jiaren Sun², Jun Zhao¹

8 ¹School of Atmospheric Sciences, Guangdong Province Key Laboratory for Climate Change and Natural
9 Disaster Studies, Southern Marine Science and Engineering Guangdong Laboratory (Zhuhai), Sun Yat-
10 sen University, Zhuhai, Guangdong 519082, China

11 ²Guangdong Province Engineering Laboratory for Air Pollution Control, Guangdong Provincial Key
12 Laboratory of Water and Air Pollution Control, South China Institute of Environmental Sciences, MEE,
13 Guangzhou 510655, China

14 ³Guangzhou Sub-branch of Guangdong Ecological and Environmental Monitoring Center, Guangzhou
15 510006, China

16 ⁴Dongguan Meteorological Bureau, Dongguan, Guangdong, 523086, China

17 ⁵Dongguan Engineering Technology Research Center of Urban Eco-Environmental Meteorology,
18 Dongguan, Guangdong, 523086, China

19 ⁶Southern Marine Science and Engineering Guangdong Laboratory (Zhuhai), Zhuhai, Guangdong
20 519082, China

21

22 *Correspondence:* Mingfu Cai (caimingfu@scies.org) and Jun Zhao (zhaojun23@mail.sysu.edu.cn)

23



24 **Abstract**

25 Understanding seasonal variation in cloud condensation nuclei (CCN) activity and the impact of
26 anthropogenic emissions in marine environments is crucial for assessing climate change. In this study,
27 two shipborne observations in the South China Sea (SCS) during the summer and winter of 2021 were
28 conducted. During summer, higher particle number concentrations but lower mass concentrations of non-
29 refractory submicron particles (NR-PM₁) were observed. These differences were attributed to the
30 dominance of particles in the Aitken mode during summer and in the accumulation mode during winter.
31 Moreover, particles during summer were more hygroscopic with higher activation ratios (ARs) at all
32 supersaturation (SS). Based on backward trajectory analysis, the whole campaign was classified into
33 terrestrial and mixed air mass influence periods. Particles measured during the terrestrial period
34 consistently exhibited lower hygroscopicity values. Additionally, minor variations were shown for all
35 NR-PM₁ components under different air mass influences during summer, while the mass fraction of
36 nitrate increased significantly under terrestrial influence during winter. Particle number size distribution
37 (PNSD) exhibited unimodal distribution during terrestrial period and bimodal distribution during mixed
38 air mass influence period, with winter displaying a more pronounced bimodal pattern than summer. The
39 impact of PNSD on AR was greater than on aerosol hygroscopicity in summer, and vice versa in winter.
40 During terrestrial period, significant variations in PNSD were observed with the offshore distance, and
41 the largest variation was seen in Aitken mode during both summer and winter. Meanwhile, aerosol
42 hygroscopicity shows an increasing trend with the offshore distance, which is primarily attributed to the
43 increase of sulfate fraction during summer and the decrease of the black carbon fraction during winter.
44 Using a single parameterized PNSD in the N_{CCN} prediction can lead to errors exceeding 100% during
45 both summer and winter, with dominant terrestrial air masses in the SCS atmosphere, while using a
46 constant hygroscopicity parameter would lower the errors in the N_{CCN} prediction (~15% during winter
47 and ~10% during summer). Our study shows significant differences in aerosol properties between winter
48 and summer seasons and highlights the influence of anthropogenic emissions on the CCN activity in the
49 SCS.

50



51 **1.Introduction**

52 Aerosols can act as cloud condensation nuclei (CCN), influencing cloud formation, lifespan, and
53 albedo, thus indirectly impacting global radiative balance (Fletcher et al., 2011; Albrecht, 1989). The
54 aerosol-cloud interaction currently represents the largest uncertainty in radiative forcing within climate
55 models, ranging from -1.7 to -0.3 W m⁻² (IPCC, 2021). This uncertainty can be attributed to the significant
56 spatiotemporal variability in the aerosol size distribution and the ability of atmospheric aerosol particles
57 acting as CCN (CCN activity) (Fitzgerald, 1973). Thus, field measurements of aerosol size distribution
58 and physicochemical properties are needed to better understand the radiative forcing exerted by
59 atmospheric aerosol particles.

60 Previous studies suggest that particle number size distribution (PNSD) is a primary factor
61 influencing CCN concentrations (Dusek et al., 2006; Rose et al., 2010; Pöhlker et al., 2016; Burkart et
62 al., 2011). The PNSD can account for 84–96% of the variability (Dusek et al. (2006) in CCN
63 concentrations (N_{CCN}), while CCN activities may also play a significant role in CCN concentrations
64 (Quinn et al., 2008; Cai et al., 2018; Ovadnevaite et al., 2017; Liu et al., 2018; Crosbie et al., 2015),
65 which are primarily governed by the particle size, chemical composition, surface tension, and
66 hygroscopicity (Köhler, 1936; Seinfeld and Pandis, 2016). Among these factors, the impact of
67 hygroscopicity on CCN activities has received great attention in recent years (Petters and Kreidenweis,
68 2007; Ajith et al., 2022; Rose et al., 2010). Petters and Kreidenweis (2007) proposed the κ - Köhler theory
69 based on the Köhler theory to quantify the ability of aerosol particles to absorb moisture and become
70 CCN based on the aerosol hygroscopicity parameters (κ). Ajith et al. (2022) showed that 64% of particles
71 can be activated as CCN when κ is equal to 0.37, whereas when κ decreases to 0.23, only 48% of particles
72 can be activated.

73 Previous field observations have indicated significant seasonal variations in PNSD and
74 hygroscopicity under both terrestrial and marine environments, leading to the seasonal variations in N_{CCN}
75 (Crosbie et al., 2015; Schmale et al., 2018; Burkart et al., 2011; Bougiatioti et al., 2009; Sihto et al., 2011;
76 Leena et al., 2016; Ross et al., 2003; Gras and Keywood, 2017; Quinn et al., 2019). Crosbie et al. (2015)
77 revealed that in the urban area of Arizona particles had larger sizes, higher hygroscopicity, and N_{CCN} was
78 also higher during winter, while a higher abundance of smaller particles was observed during summer
79 owing to stronger photochemical reactions. In pristine environments like mountain, coastal, and forested



80 regions, seasonal variations in N_{CCN} and PNSD were more pronounced than urban and rural areas
81 (Schmale et al., 2018). Pöhlker et al. (2016) observed significant differences in N_{CCN} between the wet
82 and dry seasons in the Amazon rainforest, while the κ values remained relatively stable. They also noted
83 increased particle concentrations and aerosol hygroscopicity, both subject to the impact of long-range
84 transport originating from anthropogenic emissions. Observations in marine areas during different
85 seasons are relatively scarce compared with those in inland areas. Gras (1995) found that both particle
86 concentration and N_{CCN} in the Southern Ocean reached their peaks during summer and gradually decrease
87 to their valleys in winter. Quinn et al. (2019) showed that sea spray aerosols make a relatively significant
88 contribution to N_{CCN} only during winter in the Western North Atlantic, while in other seasons, the primary
89 contribution comes from biogenic aerosols oxidized from dimethyl sulfide (DMS). Zheng et al. (2020)
90 revealed that sulfate dominates the particle condensational growth to CCN sizes during summer in the
91 North Atlantic, while secondary organic aerosols played a significant role in particle growth throughout
92 all seasons. These results indicate that CCN activity and concentration could vary in a large range during
93 different seasons. Thus, further observations across different seasons in marine environments are needed
94 to enhance our understanding of marine CCN activities and their seasonal variations.

95 The South China Sea (SCS) is located between the Asian continent to the north and the Indonesian
96 archipelago to the south. The aerosols in the SCS can be influenced by ship emissions, marine
97 background emissions, and transport of terrestrial air masses from China, Indochinese Peninsula, and
98 Philippines, making their sources relatively complex (Geng et al., 2019; Liang et al., 2021; Sun et al.,
99 2023). The complex aerosol sources in the SCS lead to the complexity of PNSD and CCN activity in this
100 area. Atwood et al. (2017) found that under the influence of marine air masses, particles exhibited a
101 significant bimodal distribution with a κ of 0.65, whereas under the influence of continental air masses,
102 a unimodal distribution and a κ of 0.4 were observed. Another summer study in the northern SCS revealed
103 a predominantly unimodal aerosol PNSD with a peak centering at 60–80 nm and an average κ value of
104 0.4 (Cai et al., 2020). Moreover, particle and N_{CCN} decreased with increasing offshore distance,
105 highlighting the significant influence of mainland China on CCN activity in the northern SCS (Cai et al.,
106 2020). However, our understanding on CCN activity, particularly the variations in CCN activity in the
107 SCS across different seasons, remains largely unknown. Conducting observational studies on CCN
108 activity across different seasons would promote our understanding of CCN activity and, ultimately,
109 reduce uncertainties related to aerosol-cloud interactions and radiative forcing in the SCS.



110 In this study, we conducted two shipborne observations in the SCS during summer (May 5–June 9,
111 2021) and winter (December 19–29, 2021). Our observations with online instruments focused on
112 measuring aerosol chemical composition, PNSD, and CCN activation in the region. Our results provide
113 valuable insights into the differences in CCN activity between winter and summer, as well as the
114 influence of terrestrial transport on CCN activity in the SCS across different seasons.

115 **2. Methodology**

116 **2.1 Cruise information and onboard measurements**

117 **2.1.1 Cruise information**

118 This study consists of two research cruises conducted during the summer and winter of 2021,
119 respectively. The summer and winter cruises were carried out respectively by the vessels "Tan Kah Kee"
120 and "Sun Yat-sen University". The "Tan Kah Kee" is an oceanographic research vessel with a length of
121 77.7 meters, a beam of 16.24 meters, and a displacement of 3611 tons. The "Sun Yat-sen University" is
122 a comprehensive oceanographic training vessel with a total length of 114.3 meters, a beam of 19.4 meters,
123 and a displacement of 6880 tons.

124 The first cruise was from May 5th to June 9th, 2021. The cruise started from Xiamen Port and
125 traversed from the northern to the central-southern South China Sea, and then circled back near Hainan
126 Island, and finally returned to Xiamen Port. The second cruise was from December 19th to December
127 29th, 2021. It began from Gaolan Port in Zhuhai and reached the vicinity of Yongxing Island, and
128 ultimately returned to Gaolan Port (Fig. 1). On both cruises, most of the instruments were housed in a
129 single compartment and the sampling lines were extended from the window of the compartment to the
130 height of the ship's bridge (Fig. S1).

131 **2.1.2 Size-resolved cloud condensation nuclei activity measurement**

132 The size-resolved CCN activity was measured with a combination of a scanning mobility particle
133 sizer (SMPS) system and a cloud condensation nuclei counter (model CCNc-200, DMT Inc., USA), the
134 SMCA method initially proposed in Moore et al. (2010). The SMPS system consisted of a differential
135 mobility analyzer (DMA; model 3082, TSI, Inc.) and a condensation particle counter (CPC; model 3756,
136 TSI Inc.). The SMPS and the CCNc system were set to measure PNSD and size-resolved CCN number



137 concentration at a mobility size range of 10–500 nm and 10–593 nm in summer and winter campaign,
138 respectively.

139 The supersaturation (SS) of the CCNc was set at 0.2 %, 0.4 %, and 0.7 % in summer campaign and
140 0.1%, 0.2 %, 0.4 %, and 0.7 % in winter campaign, respectively. Before the measurements, the CCNc
141 was calibrated with ammonium sulfate ((NH₄)₂SO₄) particles at each set SS. Detailed description of the
142 instrument configuration and calibration can be found in Cai et al. (2018).

143 **2.1.3 Aerosol chemical composition measurement**

144 The chemical composition of atmospheric non-refractory submicron particulate matter (NR-PM₁),
145 including sulfate, nitrate, organics, ammonium, and chloride, was measured using an online time-of-
146 flight ACSM (ToF-ACSM; Aerodyne Inc., USA). The sampling time of the ToF-ACSM was
147 approximately 10 min. The relative ionization efficiency (RIE) values of the instrument were calibrated
148 using ammonium nitrate (NH₄NO₃) and ammonium sulfate ((NH₄)₂SO₄) both before the start and after
149 the completion of the campaigns. The RIE values for ammonium were 3.31 and 3.33 during the summer
150 and winter, respectively, while the ones for sulfate were 1.02 and 0.81 during the summer and winter,
151 respectively. The collection efficiency (CE) was determined as shown in Sun et al. (2023) and time-
152 independent CE values were used in this study. Detailed CE calculation can be found in the
153 supplementary (Text S2). The organic carbon (OC)/elemental carbon (EC) concentrations in PM_{2.5} were
154 measured using a semi-continuous OC/EC analyzer (Model-4, Sunset Laboratory Inc., USA) based on
155 the thermal optical transmittance technique and detailed measurement process can be found in Sun et al.
156 (2023). The black carbon concentrations were measured with an aethalometer (AE33, Magee Scientific).

157 **2.1.4 Trace Gas and meteorological parameter measurements**

158 The concentrations of trace gases (CO, O₃, SO₂, and NO_x) were measured using gas monitors
159 (T400U, T100U, and T200U; Teledyne API Inc., USA). The meteorological elements, including
160 temperature, relative humidity, wind speed, and wind direction, were measured by the combined
161 automatic weather station onboard the vessels.



162 **2.2 Data analysis**

163 **2.2.1 CCN activation**

164 The size-resolved number concentration of total prarticle and cloud condensation nuclei were
165 obtained from the SMPS and CCNc through the SMCA method. The activation diameter was determined
166 by fitting the activation ratio (AR, N_{CCN}/N_{CN}) and dry diameter at each supersaturation through the
167 following equation:

168
$$\frac{N_{CCN}}{N_{CN}} = \frac{B}{1 + \left(\frac{D_P}{D_{50}}\right)^C}, \quad (1)$$

169 where D_P represents dry particle diameter (nm); B, C, and D_{50} are the three fitting parameters,
170 representing the asymptote, the slope, and the inflection point of the sigmoid, respectively (Moore et
171 al., 2010). The D_{50} parameter, also known as the critical diameter, corresponds to the particle size at
172 which 50% of the particles are activated at a specific SS.

173 The hygroscopicity parameter (κ) which represents CCN activity according to κ -Köhler equation is
174 calculated as follows (Petters and Kreidenweis, 2007):

175
$$\kappa = \frac{4A^3}{27D_{50}^3(\ln S_c)^2}, \quad A = \frac{4\sigma_{s/a}M_w}{RT\rho_w} \quad (2)$$

176 where ρ_w is the density of pure water (about 997.04 kg m⁻³ at 298.15 K), M_w is the molecular weight of
177 water (0.018 kg mol⁻¹), $\sigma_{s/a}$ corresponds to the surface tension of the solution-air interface and is assumed
178 to be equal to the surface tension of pure water ($\sigma_{s/a}$ =0.0728 N m⁻¹ at 298.15 K), R is the universal gas
179 constant (8.314 J mol⁻¹ K⁻¹), T denotes thermodynamic temperature in kelvin (298.15 K), and D_{50} is the
180 critical diameter (in m).

181 **2.2.2 CCN concentration and activation ratio calculation**

182 The CCN concentration (N_{CCN}) can be predicted based on particle number size distribution (PNSD)
183 and D_{50} at a specific SS. It can be calculated by the following equation (Cai et al., 2018):

184
$$N_{CCN}(SS) = \int_{D_{50}(SS)}^{\infty} N_{CN}(D_P) dD_P \quad (3)$$

185 where $N_{CCN}(SS)$ is CCN concentration at a specific SS, $D_{50}(SS)$ is the activation diameter at a specific
186 SS from the SMCA method and $N_{CN}(D_P)$ is the particle number concentration under specific diameter
187 from SMPS measurement.

188 The AR can be calculated by:



$$189 \quad AR = \frac{\int_{D_{50}(SS)}^{\infty} N_{CN}(DP) dDP}{\int_0^{\infty} N_{CN}(DP) dDP} \quad (4)$$

190 To investigate the effect of PNSD and D_{50} on N_{CCN} and AR, we defined delta N_{CCN} (ΔN_{CCN}) and
191 delta AR (ΔAR). They are calculated by following equations:

$$192 \quad \Delta N_{CCN} = \frac{N_{CCN, sim} - N_{CCN, actual}}{N_{CCN, actual}} \quad (5)$$

$$193 \quad \Delta AR = \frac{N_{CCN, actual} - N_{CCN, sim}}{N_{CCN, actual}} \quad (6)$$

194 The subscript "actual" represents the actual measured value, while the subscript "sim" represents the
195 simulated value.

196 2.2.3 Primary and secondary organic carbon concentration calculation

197 The concentrations of primary organic carbon (POC) and secondary organic carbon (SOC) were
198 calculated according to following equation:

$$199 \quad POC = (OC/EC)_{pri} \times EC \quad (7)$$

$$200 \quad SOC = OC_{total} - (OC/EC)_{pri} \times EC \quad (8)$$

201 where $(OC/EC)_{pri}$ is the OC/EC ratio in freshly emitted combustion aerosols, and OC_{total} and EC are
202 available from ambient measurements. The $(OC/EC)_{pri}$ was obtained from the minimum R squared (MRS)
203 method (Wu and Yu, 2016). The MRS approach provides more accurate estimation of SOC than
204 $(OC/EC)_{min}$ or $(OC/EC)_{10\%}$ approach and the results obtained from the MRS method are sensitive to the
205 magnitude of measurement uncertainty, but the bias does not exceed 23% if the uncertainty is within 20%
206 (Wu and Yu, 2016). In this study, the $(OC/EC)_{pri}$ values were 3.65 and 0.25 in summer when affected by
207 terrestrial air masses and terrestrial-marine mixed air masses, while they were 2.82 and 0.82 in winter
208 when affected by terrestrial air masses and terrestrial-marine mixed air masses, respectively. The
209 categorization method based on the influence of different air masses will be introduced in the next section.

210 2.2.4 Backward trajectory simulation

211 Backward trajectory calculations were performed using MeteoInfo, an open-source software (Wang,
212 2014) to determine potential source origins. Weekly GDAS1 (Global Data Assimilation System at a
213 resolution of 1°) files were downloaded from the NOAA Air Resource Laboratory (ARL) website
214 (<https://www.ready.noaa.gov/gdas1.php>). The calculation of backward trajectories is performed every 12



215 hours based on the location of the ship, generating 48-hour backward trajectories at 50m, 150m, 500m,
216 and 1000m heights.

217 **3. Results and discussion**

218 **3.1 Overview**

219 Figure 2 shows the timeseries of PNSD (a1 and a2), PM₁ mass concentrations and fractions (b1 and
220 b2, c1 and c2), number concentrations of CCN (d1 and d2), and hygroscopicity κ -values (e1 and e2)
221 during two campaigns in summer and winter. Based on the backward trajectories and source origins, both
222 campaigns were classified into two periods: the period influenced by terrestrial-marine mixed air masses
223 (31%) and the period influenced by terrestrial air masses only (69%) (Fig. S3). During the summer,
224 terrestrial air masses primarily traverse through the Philippines region, whereas during the winter, they
225 predominantly originate from mainland China. As shown in Fig. 2, a higher total particle number
226 concentration during summer (11195 cm⁻³) than during winter (6358 cm⁻³) was obtained when the marine
227 atmosphere was mainly influenced by terrestrial air masses. This is in line with previous studies that a
228 higher particle number concentration of exceeding 15000 cm⁻³ was observed in Manila (the largest port
229 city in the Philippines) than that of approximately 10000 cm⁻³ reported in Guangzhou and Hong Kong
230 (Liu et al., 2008; Cai et al., 2017). Similar particle concentrations (2114 cm⁻³ and 1840 cm⁻³) in winter
231 and summer were shown when the marine atmosphere was predominantly influenced by mixed air
232 masses. Interestingly, they are much lower than those (~3400 cm⁻³) observed in the northern South China
233 Sea (Cai et al., 2020), but higher than those observed in the remote SCS (975 cm⁻³) when similar mixed
234 influences of air masses (Atwood et al., 2017).

235 The average mass concentration of NR-PM₁ was 3.60 $\mu\text{g m}^{-3}$ in summer and significantly increased
236 to 18.11 $\mu\text{g m}^{-3}$ in winter. However, this summer concentration was much lower than the concentrations
237 (9.11 $\mu\text{g m}^{-3}$ and 10.65 $\mu\text{g m}^{-3}$) measured in similar summer periods of 2018 and 2019 in the northern
238 SCS (Liang et al., 2021; Sun et al., 2023). As aforementioned, the particle number concentrations were
239 higher in summer than in winter when the atmosphere was primarily influenced by terrestrial air masses.
240 However, the particles in summer were predominantly in the Aitken mode, resulting in a lower
241 contribution to the mass loading than those in winter which were mainly in the accumulation mode (Fig.
242 3). Additionally, higher NR-PM₁ concentrations were found in both summer and winter under the



243 influence of terrestrial air masses than mixed ones, with decreases of approximately $0.6 \mu\text{g m}^{-3}$ (from
244 3.84 to $3.20 \mu\text{g m}^{-3}$) and $17 \mu\text{g m}^{-3}$ (from 23.52 to $6.32 \mu\text{g m}^{-3}$) in summer and winter, respectively. The
245 dramatic decrease for the latter case indicated a more pronounced impact of inland anthropogenic
246 emissions on the aerosol mass concentration in the SCS region during winter.

247 As shown in Fig. 2 (d1 and d2), the N_{CCN} values at three supersaturation levels (0.2%, 0.4%, and
248 0.7%) in winter (1660, 2356, and 3053 cm^{-3}) were lower than those in summer (2899, 5450, and 5770
249 cm^{-3}), respectively. Specifically, the N_{CCN} (5450 cm^{-3}) at 0.4% SS in this study during summer is much
250 higher than that (1544 cm^{-3}) measured at a similar SS (0.34%) in summer 2018 in the similar northern
251 SCS region (Cai et al., 2020). This is primarily due to most of the particles being in the Aitken mode
252 particles during summer (Figs. 3a and c). For comparison, the average total particle number concentration
253 in summer is twice that in winter, however, no such a significant difference in CCN concentration was
254 seen.

255 The median values of κ were approximately 0.5 in summer and 0.3 in winter (Fig. 2e), respectively.
256 During summer, the median κ value was slightly higher than that (~ 0.4) measured in 2018 in the similar
257 northern SCS (Cai et al., 2020), but lower than that (0.65) in the southern SCS (Atwood et al., 2017).
258 Comparatively, under the influence of terrestrial air masses, the κ values ranged from 0.41 to 0.50 (Fig.
259 3a), close to the above value of 0.4 in 2018 (Cai et al., 2020). Furthermore, under the influence of mixed
260 air masses, the κ values ranged from 0.49 to 0.61 (Fig. 3c), similar to those observed in the southern SCS
261 (0.54) and the Western North Pacific (0.49–0.64), but lower than those in the southern SCS (0.65) and
262 the Western North Pacific (0.48–0.84) under the influence of marine air masses (Atwood et al., 2017;
263 Kawana et al., 2022). During winter, under the influence of terrestrial air masses, the κ values ranged
264 from 0.17 to 0.38 (Fig. 3b), very close to those (0.14–0.37) measured in Guangzhou (Fig. 3d) (Cai et al.,
265 2018). This specific winter scenario indicates that aerosols in the northern SCS are significantly
266 influenced by the air masses transported from the mainland China during winter season. Compared to
267 terrestrial air masses, the κ values were respectively higher at the set SS under the influence of mixed air
268 masses (Fig. 3d). The above differences on hygroscopicity are likely attributed to variations in aerosol
269 chemical composition during different seasons and under the influence of different air masses. In both
270 winter and summer, the PNSD exhibits a unimodal distribution under the influence of terrestrial air
271 masses, while it shows a bimodal distribution under the influence of mixed air masses (Fig. 3). The
272 bimodal distribution may result from a mixture of particles from marine primary emissions and from



273 transported anthropogenic emissions across the region, while the unimodal distribution was primarily
274 composed of particles from inland-transported anthropogenic emissions (Frossard et al., 2014; Atwood
275 et al., 2017).

276 **3.2 Impact of chemical composition on hygroscopicity**

277 Chemical composition is a crucial factor influencing aerosol hygroscopicity due to distinct
278 hygroscopic properties exhibited by each chemical component (Petters and Kreidenweis, 2007). We
279 observed two significant differences in aerosol hygroscopicity between summer and winter (Fig. 3).
280 Firstly, aerosol hygroscopicity was considerably higher in summer than that in winter. Secondly, aerosol
281 hygroscopicity under terrestrial-influencing air masses was lower than that under mixed-influencing air
282 masses. Additionally, hygroscopicity decreased with increasing particle size in summer, whereas
283 opposite effect was observed in winter. In this section, we primarily discuss the differences in aerosol
284 hygroscopicity between summer and winter, as well as the variations observed when influenced by
285 different air masses, from the chemical composition perspective.

286 **3.2.1 Impact of inorganic components**

287 In summer, the highest proportion of NR-PM₁ components measured by ACSM is sulfate (40.3%),
288 followed by organic (37.3%), ammonium (14.0%), nitrate (6.2%), and chloride (2.3%) (Fig. 4). However,
289 in winter, organic (39.2%) has the highest proportion, followed by nitrate (22.1%), sulfate (19.5%),
290 ammonium (17.7%), and chloride (1.5%) (Fig. 4). Compared to summer, the significant increase of
291 nitrate proportion and decrease of sulfate in winter were mainly attributed to the difference in air masses.
292 Winter terrestrial air masses originate from mainland China and primarily pass through the PRD region
293 to reach the South China Sea, while the summer ones primarily originate from the Philippines region.
294 Stronger transportation and industrial emissions in the PRD than in the Philippines lead to higher NO_x
295 concentrations and hence higher nitrate concentrations (Wang et al., 2019). A high proportion of nitrate
296 sulfate in the PRD during winter was previously reported in NR-PM₁ (Yang et al., 2022), whereas sulfate
297 was found the major component in the Philippines (Tseng et al., 2019).

298 Previous studies showed that nitrate has slightly higher hygroscopicity than sulfate (Gysel et al.,
299 2007; Topping et al., 2005). For example, the κ values for ammonium sulfate ((NH₄)₂SO₄), ammonium
300 bisulfate (NH₄HSO₄), and ammonium nitrate (NH₄NO₃) are 0.48, 0.56, and 0.58, respectively (Huang et



301 al., 2022). In some marine environments, aerosols exhibit a high acidity with low ammonium
302 concentrations, where sulfate and nitrate primarily exist in the form of sulfuric acid (H_2SO_4 , κ : 0.7) and
303 nitric acid (HNO_3 , κ : 0.85), respectively, thereby enhancing aerosol hygroscopicity (Chang et al., 2011;
304 Siegel et al., 2022). Here, we use the ratio of NH_4^+ (measured) to NH_4^+ (predicted) to roughly determine
305 an aerosol being “acidic” or “alkaline” (Guo et al., 2015): more acidic if this ratio is smaller one because
306 the imbalance indicates the possible presence of acidic compounds such as H_2SO_4 , HNO_3 , or HCl in the
307 aerosol (Zhang et al., 2021). The median values of this ratio in summer and winter are 0.82 and 1.11,
308 respectively, exceeding the threshold of 0.75 (Fig. S5), a rough estimate for equal molecular numbers of
309 $(\text{NH}_4)_2\text{SO}_4$ and NH_4HSO_4 . This indicates that sulfate and nitrate are primarily present in the form of
310 $(\text{NH}_4)_2\text{SO}_4$ and NH_4NO_3 both in summer and winter in the SCS. Since the hygroscopicity values of
311 $(\text{NH}_4)_2\text{SO}_4$ and NH_4NO_3 are similar, changes in their proportions may not be the primary driver of the
312 observed aerosol hygroscopicity variations between winter and summer. Interestingly, we found that the
313 mass concentrations of BC and EC were higher in winter ($1.79 \mu\text{g m}^{-3}$ and $1.16 \mu\text{g m}^{-3}$) than those in
314 summer ($0.61 \mu\text{g m}^{-3}$ and $0.64 \mu\text{g m}^{-3}$), which might be one of the reasons for the lower aerosol
315 hygroscopicity in winter because of the hydrophobicity nature of BC ($\kappa=0$) (Weingartner et al., 1997;
316 Siegel et al., 2022). Another reason may be attributed to the hygroscopicity variations of organic
317 components (κ_{org}), which will be discussed in the following section.

318 As introduced at the beginning of the section, the hygroscopicity decreased with increasing particle
319 size during summer, in contrast to the increasing trend during winter, which may be attributed to the
320 oxidation of dimethyl sulfide (DMS). DMS oxidation produces methanesulfonic acid (MSA) which is
321 further oxidized to form non-sea salt (NSS) sulfate in smaller particles (Raes et al., 2000). The ratio of
322 sulfate to MSA (SA/MSA) can be used to assess the impact of DMS oxidation and anthropogenic
323 emissions on sulfate (Savoie et al., 2002; Zhang et al., 2007; Cai et al., 2020). A lower ratio indicates a
324 more significant influence of DMS oxidation on sulfate, while a higher ratio suggests a greater influence
325 of anthropogenic emissions. Previous studies have found that SA/MSA is approximately 15–625 in the
326 northern South China Sea region, significantly higher than that (18–20) in the open ocean (Zhang et al.,
327 2007; Savoie et al., 2002). Cai et al. (2020) reported this ratio in a range of 100–10000 using Modern-
328 Era Retrospective analysis for Research and Applications, Version 2 (MERRA-2) reanalysis data in a
329 similar northern SCS region. In this study, since we could not accurately distinguish MSA from other



330 organic components using ToF-ACSM due to its low mass resolution, we employed the same method to
331 analyze the SA/MSA distribution in the South China Sea region during the observation period (Fig. S6).
332 Our results showed that this ratio ranged from approximately 100 to 3000 in summer, whereas it exceeded
333 10000 in winter, indicating a greater impact of anthropogenic emissions than DMS oxidation on the NSS
334 sulfate in the SCS, with a more pronounced influence in winter than in summer. Higher DMS
335 concentrations in summer than in winter are likely due to higher sea surface temperatures which promote
336 the production rate of DMS by phytoplankton (Bates et al., 1987). Therefore, it is likely that there is a
337 higher amount of NSS sulfate produced through DMS oxidation during summer, contributing to the
338 sulfate production and hence increasing aerosol hygroscopicity in smaller particles during summer.

339 3.2.2 Impact of organic components

340 The mass concentrations of organics exhibit significant differences between winter ($7.15 \mu\text{g m}^{-3}$)
341 and summer ($1.34 \mu\text{g m}^{-3}$), while the total fractions in NR-PM₁ remain relatively consistent (40% and
342 37% in winter and summer, respectively). Despite their similar proportions in winter and summer, the
343 differences in the organic components may likely play an important role in the variations of
344 hygroscopicity. Previous studies showed that the measured hygroscopic parameter was linearly
345 correlated with the organic mass fraction (f_{org}) (Bhattu et al., 2016; Huang et al., 2022; Dusek et al., 2010).
346 Here, we employed linear regression to relate κ obtained at 0.2% SS ($\kappa_{\text{ss}:0.2\%}$) to f_{org} measured by ToF-
347 ACSM (Fig. 5). Two reasons for choosing $\kappa_{\text{ss}:0.2\%}$: (1) It represents hygroscopicity of larger particles
348 (~ 100 nm) than that at higher SSs. (2) The κ values at 0.1% SS ($\kappa_{\text{ss}:0.1\%}$) is only available in winter. In
349 addition, the measured mass concentrations focused on larger particles which were represented by those
350 of $\kappa_{\text{ss}:0.2\%}$. We consider κ as hygroscopicity of organics (κ_{org}) when f_{org} approaches 1 and as that of
351 inorganics (κ_{inorg}) when f_{org} is nearly 0.

352 During summer and winter under the influence of terrestrial air masses, the κ_{org} value was
353 approximately 0.09, while under the influence of mixed air masses, it was approximately 0.21 and 0.20,
354 respectively. This result suggests that no significant differences of κ_{org} were found between summer and
355 winter under the same influence of air masses. However, pronounced differences of κ_{org} were indeed
356 observed under the influence of different air masses which may be associated with different types of
357 organic compounds responsible for hygroscopicity. This was further supported by variations of the POC
358 and SOC fractions. In general, POC is associated with primary organic aerosol (POA), primarily



359 originating from combustion sources, such as fossil fuel, biomass burning, and biogenic emissions, while
360 SOC is associated with secondary organic aerosol (SOA), primarily originating from the oxidation of
361 POA (Wu and Yu, 2016). In addition, SOC exhibits higher hygroscopicity than POC (Jayachandran et
362 al., 2022; Safai et al., 2014). Previous studies have indicated that highly aged organic compounds exhibit
363 higher hygroscopicity than the less oxidized counterparts (Lambe et al., 2011; Jimenez et al., 2009).
364 Previous studies showed that the κ_{org} values are in a range of 0.02–0.17 when the O/C ratio varies from
365 0.2 to 0.6 (Jimenez et al., 2009) and κ_{POA} (κ corresponds to POA, similar to κ_{org}) and κ_{SOA} are respectively
366 in the ranges of 0–0.1 and 0.1–0.3 due to different types of organic aerosol (Liu and Wang, 2010; Kuang
367 et al., 2020). A higher proportion of POC was observed during the terrestrial periods, whilst a significant
368 increase in the fraction of SOC was shown under the influence of mixed air masses (Figs. 4 h-m). As a
369 result, the increasing oxidation degree of SOA and the decreasing proportion of POA lead to higher κ_{org}
370 under mixed air masses than those under continental air masses. This is also consistent with a recent
371 study in the SCS (Sun et al., 2023), revealing that a combined effect of photo-oxidation and liquid-phase
372 reactions play an essential role in the BBOA aging processes.

373 **3.3 Differences in the CCN activation ratio during different seasons**

374 The CCN activation ratio (AR), which quantifies the number fraction of aerosol particles capable
375 of acting as CCN at a specific supersaturation level, is an important parameter for characterizing the
376 CCN activity (Dusek et al., 2006). In addition, AR is also a useful parameter in the CCN prediction
377 (Pruppacher, 2010; Deng et al., 2013). Figure 6 illustrates the variations in AR and N_{CCN} under the
378 influence of different air masses during different seasons. The median AR values were higher in summer
379 (0.39, 0.67, and 0.85 at 0.2%, 0.4%, and 0.7% SS, respectively) than in winter (0.21, 0.36, 0.49, and 0.64
380 at 0.1%, 0.2%, 0.4%, and 0.7% SS, respectively). In summer under terrestrial air masses, the ARs (0.34–
381 0.81 at 0.2%–0.7% SS) in this study were lower than those (0.49–0.85 at 0.18%–0.59% SS) in a previous
382 study in the same region (Cai et al., 2020), but higher than those (0.18–0.48 at 0.11%–0.60% SS) in the
383 Western North Pacific (Kawana et al., 2022). However, under mixed air masses, the AR values were
384 higher than those (0.31–0.71 at 0.18%–0.59% SS) reported in Cai et al. (2020) and close to those (0.42–
385 0.85 at 0.11%–0.60% SS) in the Western North Pacific (Kawana et al., 2022). In winter under terrestrial
386 air masses, the AR values were in a range of 0.14 to 0.59 at 0.1%–0.7% SS, consistent with those



387 measured in the Guangzhou (0.26–0.64 at 0.1%–0.7% SS) and Hong Kong (0.16–0.65 at 0.15%–0.7%
388 SS) (Cai et al., 2018; Meng et al., 2014).

389 The differences of AR between different seasons under different air masses could be attributed to
390 different PNSD and hygroscopicity. When the PNSD concentrates particles in the size range beyond the
391 D_{50} , more particles can be activated as CCN, leading to higher ARs. Meanwhile, more hygroscopic
392 particles intend to have smaller D_{50} values with which more particles can be activated. Previous studies
393 showed that the influence of the above two factors may vary under different environments. The PNSD
394 played a more important role in most cases in continental area (Dusek et al., 2006; Tao et al., 2021), while
395 hygroscopicity can also have significant effects in some environments, such as boreal forest and coastal
396 area (Roldin et al., 2019; Bougiatioti et al., 2016). Here, we investigate the relative importance of aerosol
397 PNSD and chemical composition (hence hygroscopicity) in the SCS during different seasons under
398 different air masses. We define ΔAR as the difference between the actual and estimated AR using Eq.
399 (7), following a procedure illustrated in Fig. S8. AR was calculated using Eq. (4) based on the average
400 D_{50} and the PNSD obtained during different seasons and periods (Fig. S8). Figure 7 shows that the ΔAR
401 values at 0.2%–0.7% SS between summer and winter due to D_{50} were from -22% to 29%, while they
402 were from -10% to 12% due to PNSD, indicating more significant influence of D_{50} than PNSD on N_{CCN} ,
403 in the South China. In fact, the peak diameters of PNSD during both winter and summer are around 70
404 nm, and their variations are relatively small compared to the changes in D_{50} (Fig. S9).

405 We further investigate the influence of PNSD and hygroscopicity on AR under different air masses
406 in the same season. In summer, the influence of PNSD on the AR can reach 6.0% to 9.8% between
407 different periods (Figs. 7 b1 and c1), with the most significant impact at 0.2% SS ($D_{50} > 90$ nm). This
408 can be attributed to the fact that large variations in accumulation mode particles significantly impact AR
409 with peaking at a larger size for terrestrial air masses (151 nm) than mixed air masses (140 nm) (Figs. S9
410 a1-a3). In comparison, the impact of hygroscopicity (based on D_{50}) on AR is relatively small, for example,
411 the influence is estimated to be around 1.3%–3.4% at 0.2% and 0.7% SS, and ~6% at 0.4% SS. In winter,
412 the impact of hygroscopicity on AR at all SS levels (2.6%–5.1%) was more significant than that of PNSD
413 (1.2%–3.2%) (Fig. 7). We attribute this difference to two possible reasons: (1) Particles tend to be more
414 concentrated in larger sizes (Fig. S9) and the changes in PNSD under different air masses have a
415 relatively minor impact on AR. (2) the D_{50} values in winter are larger than those in summer and are closer



416 to the peak sizes of the PNSD (Figs. S9 b1-b3). The results suggest that PNSD was the most important
417 factor influencing N_{CCN} in summer, while hygroscopicity became more important in winter.

418 **3.4 Influence of spatial distribution of particle properties on N_{CCN}**

419 This section focuses on how the spatial distribution of aerosol concentration and physicochemical
420 properties influences CCN concentrations under different air masses, particularly the variations occurring
421 with offshore distance. Typically, N_{CCN} in a specific region is predicted in models with a single
422 parameterized PNSD and it can be used to simulate the hygroscopic growth process (Yu and Luo, 2009).
423 Here, we further investigated the impact of spatial variations in PNSD and hygroscopicity on the
424 prediction of N_{CCN} . In summer, terrestrial air masses primarily pass through the Philippines and the
425 impact varies with longitude, while during winter, terrestrial air masses are predominantly from mainland
426 China, especially the PRD region, and the impact varies with latitude (Fig. S3). Hence, we investigate
427 the influence in summer based on longitude and in winter based on latitude. Figure 8 illustrates the
428 variations of the N_{CCN} and number concentration of different mode particles, κ at 0.4% SS ($\kappa_{SS:0.4\%}$), the
429 ratio of SOC to OC, mass concentration of BC, and NR-PM₁ component proportions with increasing
430 offshore distance.

431 In summer, the N_{CCN} showed a decreasing trend with increasing offshore distance under the
432 terrestrial air masses, while no significant variation was observed under the mixed air masses.
433 Furthermore, the number concentration of Aitken mode particles significantly decreased with increasing
434 offshore distance (from 118°E to 113°E), from nearly 10^4 to approximately 10^3 (Fig. 8a2). Similarly, the
435 number concentration of accumulation mode particles exhibited a decreasing trend. In contrast, no
436 significant variation was observed for the number concentration of nucleation mode particles, indicating
437 that those particles were less affected by the terrestrial air masses. The $\kappa_{SS:0.4\%}$ values exhibit an increasing
438 trend with increasing offshore distance under the terrestrial air masses, while no obvious trend was shown
439 under the mixed air masses (Figs. 8 a3 and b3). The above observations can be attributed to three possible
440 reasons: (1) A higher degree of oxidation for the organic component enhances the hygroscopicity of the
441 particles, as evidenced by the increasing trend of the SOC/OC ratio with increasing offshore distance
442 (0.4 to 0.7 from 118°E to 113°E, Fig. 8a4). (2) A significant decrease in the BC concentration (0.5 to 0.3
443 $\mu\text{g m}^{-3}$ from 118°E to 113°E, Fig. 8a5) may contribute to an increase of the aerosol hygroscopicity. (3)
444 An increase of sulfate fraction with increasing offshore distance may lead to a decrease of organic



445 compounds (Fig. 8a6). The increase of hygroscopicity with increasing offshore distance lowered the D_{50}
446 values and led to the increase of N_{CCN} , while the decrease of N_{CCN} was primarily attributed to the change
447 of the particle concentrations in Aitken mode and accumulation mode.

448 In winter, the increasing trend with increasing offshore distance is similar to that in summer under
449 the terrestrial air masses, while no significant N_{CCN} variation was observed under the mixed air masses
450 (Figs. 8c1-c2 and d1-d2). Meanwhile, the aerosol hygroscopicity exhibits a slight increasing trend with
451 offshore distance (a κ value of 0.19 to 0.21 from 22°N to 19°N). The increase of aerosol hygroscopicity
452 with increasing offshore distance can be explained by two possible reasons: (1) The nitrate mass fraction
453 decreased significantly and organics became the predominant component with increasing offshore
454 distance. Hence, the increased oxidation degree of the organic component was an important factor for
455 the enhancement of aerosol hygroscopicity which is supported by the increase of the SOC/OC ratio (Fig.
456 8c4). (2) The decrease of the BC concentrations with increasing offshore distance was more pronounced
457 during winter (2.1 to $0.6 \mu\text{g m}^{-3}$) than during summer (0.5 to $0.3 \mu\text{g m}^{-3}$), indicating that the decrease of
458 the BC mass fraction is also a significant contributor to the overall increase of aerosol hygroscopicity.
459 Interestingly, the slight decrease of the average κ value further offshore (19°N to 20°N) was caused by
460 the impact of nearby ship emissions which was further supported by the decrease of SOC/OC ratio.

461 The impact of spatial distribution of D_{50} and PNSD on N_{CCN} was further investigated through
462 calculating N_{CCN} using D_{50} or PNSD (Eq. (3)) according to the scheme shown in Fig. S10. For example,
463 to investigate the impact of PNSD on N_{CCN} , the PNSD which are closest and furthest from the shore and
464 the observed D_{50} were used to calculate N_{CCN} . Here, we define ΔN_{CCN} as the ratio of the difference
465 between calculated N_{CCN} and observed N_{CCN} , divided by the observed N_{CCN} (Eq. (7)). However, under
466 the mixed air masses, as mentioned above, since no obvious variations of PNSD and aerosol
467 hygroscopicity with offshore distance were observed (Figs. 8 b2-b3 and d2-d3), the impact of spatial
468 distribution of D_{50} and PNSD on N_{CCN} was less significant (Fig. S11). Hence, below we only discuss the
469 scenarios under the terrestrial air masses.

470 Figure 9 shows ΔN_{CCN} at different offshore distances under the terrestrial air masses. In summer, a
471 monotonic trend of ΔN_{CCN} was observed with a value of up to approximately 70% at 0.2 SS under the
472 effect of hygroscopicity. In winter, the impact of hygroscopicity was less pronounced than that in summer,
473 reaching only up to around 10% (Figs. 9 c1 and c2). This indicates that a single hygroscopicity parameter



474 can represent the overall hygroscopicity in SCS under the influence of terrestrial air masses in winter,
475 whereas during summer, this approach may not be sufficient. The ΔN_{CCN} nearshore caused by the impact
476 of PNSD can exceed 300% and can reach up to 80% furthest offshore during summer, indicating that the
477 spatial distribution of PNSD has a greater impact on N_{CCN} than hygroscopicity. Similarly, although the
478 impact was less significant during winter, the ΔN_{CCN} nearshore can still reach 80% (Fig. 9 d1 and d2).
479 Hence, in summary, using a single PNSD for the representation of PNSD in the region of SCS can lead
480 to significant uncertainties in the prediction of N_{CCN} under the terrestrial air masses during both summer
481 and winter.

482 4. Conclusion

483 In this study, we investigated the seasonal variations of CCN activity in the SCS and explored the
484 impact of anthropogenic emissions, based on shipborne observations conducted during the summer (May
485 5–June 9) and winter (December 19–29) of 2021. CCN activity, chemical composition, and particle
486 number size distribution (PNSD) over the SCS were measured using several onboard instruments
487 including a ToF-ACSM, a CCNc, an SMPS, an OC/EC analyzer, an AE33, and several monitors for trace
488 gases (i.e., SO_2 , NO_x , CO, and O_3). Our results show that the particle number concentration (N_{CN}) and
489 CCN number concentration (N_{CCN}) during summer were higher than those during winter, while the NR-
490 PM_1 mass concentration was lower in summer, which can be attributed to the predominance of the Aitken
491 mode particles in summer than a significant higher concentration of the accumulation mode particles
492 during winter. Additionally, the aerosol hygroscopicity was found to be higher in summer than in winter,
493 likely due to the enhanced terrestrial air masses and the increased proportions of black carbon and
494 decreased sulfate concentrations from DMS oxidation.

495 Based on backward trajectories, both campaigns could be divided into two periods: period affected
496 by terrestrial air masses and period affected by both terrestrial and marine (mixed) air masses. In summer,
497 the terrestrial air masses originate primarily from the Philippines, whereas in winter, they predominantly
498 originate from the PRD region of China. The hygroscopicity under terrestrial air masses was lower than
499 that under mixed air masses during both seasons, and it was similar to that observed in the PRD region
500 during winter. The PNSD distribution exhibited a unimodal pattern under the terrestrial air masses,
501 whereas a bimodal pattern was observed under the mixed air masses. During winter, the N_{CCN} values



502 were higher under terrestrial air masses in contrast to higher AR values under mixed air masses. During
503 summer, the AR ratio was primarily influenced by PNSD, whereas during winter, it was more strongly
504 influenced by aerosol hygroscopicity than by PNSD.

505 Our study demonstrated significant variations in the aerosol concentration and physicochemical
506 properties with increasing offshore distances under terrestrial air masses during both summer and winter.
507 The decreasing trends observed in various gas concentrations (NO_x and CO) with increasing offshore
508 distances suggest a diminishing influence of anthropogenic emissions. The aerosol hygroscopicity
509 increased with increasing offshore distances, primarily due to the decrease of the organic fraction, the
510 oxidation degree of the organic component, the decreased proportions of black carbon, and the increased
511 sulfate ratio. We found that the predicted CCN concentrations nearshore based on a single PNSD under
512 terrestrial air masses could lead to significant error (15%–360%). In contrast, using a representative
513 hygroscopicity parameter value nearshore can reduce the error in predicting N_{CCN} (5%–10%). Hence, the
514 PNSD had a greater impact on N_{CCN} prediction than hygroscopicity. Our study highlights the significant
515 differences of CCN activity during summer and winter in the SCS and significant influence of
516 anthropogenic emissions on the CCN activity. Future studies should include observations during spring
517 and autumn to explore the impact of mixing state on aerosol hygroscopicity for a more comprehensive
518 understanding of CCN activity in this region.

519

520 *Data availability.* Data from the measurements are available at
521 <https://doi.org/10.6084/m9.figshare.25472545> (Ou et al., 2024).

522

523 *Supplement.* The supplement related to this article is available online at xxx.

524

525 *Author contributions.* **HO, MC, and JZ** designed the research. **YZ, XN, BL, and CS** performed the
526 measurements. **HO, MC, QS, and SM** analyzed the data. **SZ and HW** provided useful comment on the
527 paper. **HO, MC, and JZ** wrote the paper with contributions from all co-authors.

528

529 *Competing interests.* The authors declare that they have no conflict of interest.

530



531 *Financial support.* This work was supported by National Natural Science Foundation of China (NSFC)
532 (Grant No. 42305123 and 42175115) and Basic and Applied Basic Research Foundation of Guangdong
533 Province (Grant No. 2023A1515012240).

534

535 *Acknowledgements.* Additional support from the crew of the vessels "Tan Kah Kee" and "Sun Yat-sen
536 University" is greatly acknowledged.

537

538



539 **Reference**

- 540 Ajith T. C, Kompalli, S. K., and Babu, S. S.: Role of Aerosol Physicochemical Properties on Aerosol
541 Hygroscopicity and Cloud Condensation Nuclei Activity in a Tropical Coastal Atmosphere, ACS Earth
542 Space Chem, 6, 1527-1542, doi:<https://doi.org/10.1021/acsearthspacechem.2c00044>, 2022.
- 543 Albrecht, B. A.: Aerosols, cloud microphysics, and fractional cloudiness, Science, 245, 1227-1230,
544 doi:<https://doi.org/10.1126/science.245.4923.1227>, 1989.
- 545 Atwood, S. A., Reid, J. S., Kreidenweis, S. M., Blake, D. R., Jonsson, H. H., Lagrosas, N. D., Xian, P.,
546 Reid, E. A., Sessions, W. R., and Simpas, J. B.: Size-resolved aerosol and cloud condensation nuclei
547 (CCN) properties in the remote marine South China Sea - Part 1: Observations and source classification,
548 Atmos. Chem. Phys., 17, 1105-1123, doi:<https://doi.org/10.5194/acp-17-1105-2017>, 2017.
- 549 Bates, T. S., Cline, J. D., Gammon, R. H., and Kelly-Hansen, S. R.: Regional and seasonal variations in
550 the flux of oceanic dimethylsulfide to the atmosphere, J. Geophys. Res. Oceans, 92, 2930-2938,
551 doi:<https://doi.org/10.1029/JC092iC03p02930>, 1987.
- 552 Bhattu, D., Tripathi, S. N., and Chakraborty, A.: Deriving aerosol hygroscopic mixing state from size-
553 resolved CCN activity and HR-ToF-AMS measurements, Atmos Environ, 142, 57-70,
554 doi:<https://doi.org/10.1016/j.atmosenv.2016.07.032>, 2016.
- 555 Bougiatioti, A., Fountoukis, C., Kalivitis, N., Pandis, S. N., Nenes, A., and Mihalopoulos, N.: Cloud
556 condensation nuclei measurements in the marine boundary layer of the eastern Mediterranean: CCN
557 closure and droplet growth kinetics, Atmos. Chem. Phys., 9, 7053-7066, doi:<https://doi.org/10.5194/acp-9-7053-2009>, 2009.
- 559 Bougiatioti, A., Bezantakos, S., Stavroulas, I., Kalivitis, N., Kokkalis, P., Biskos, G., Mihalopoulos, N.,
560 Papayannis, A., and Nenes, A.: Biomass-burning impact on CCN number, hygroscopicity and cloud
561 formation during summertime in the eastern Mediterranean, Atmospheric Chemistry and Physics, 16,
562 7389-7409, doi:<https://doi.org/10.5194/acp-16-7389-2016>, 2016.
- 563 Burkart, J., Steiner, G., Reischl, G., and Hittenberger, R.: Long-term study of cloud condensation nuclei
564 (CCN) activation of the atmospheric aerosol in Vienna, Atmos Environ, 45, 5751-5759,
565 doi:<https://doi.org/10.1016/j.atmosenv.2011.07.022>, 2011.
- 566 Cai, M., Tan, H., Chan, C. K., Mochida, M., Hatakeyama, S., Kondo, Y., Schurman, M. I., Xu, H., Li, F.,
567 Shimada, K., Li, L., Deng, Y., Yai, H., Matsuki, A., Qin, Y., and Zhao, J.: Comparison of Aerosol



568 Hygroscopicity, Volatility, and Chemical Composition between a Suburban Site in the Pearl River Delta
569 Region and a Marine Site in Okinawa, *Aerosol Air Qual Res*, 17, 3194-3208,
570 doi:<https://doi.org/10.4209/aaqr.2017.01.0020>, 2017.

571 Cai, M. F., Liang, B. L., Sun, Q. B., Zhou, S. Z., Chen, X. Y., Yuan, B., Shao, M., Tan, H. B., and Zhao,
572 J.: Effects of continental emissions on cloud condensation nuclei (CCN) activity in the northern South
573 China Sea during summertime 2018, *Atmos. Chem. Phys.*, 20, 9153-9167,
574 doi:<https://doi.org/10.5194/acp-20-9153-2020>, 2020.

575 Cai, M. F., Tan, H. B., Chan, C. K., Qin, Y. M., Xu, H. B., Li, F., Schurman, M. I., Liu, L., and Zhao, J.:
576 The size-resolved cloud condensation nuclei (CCN) activity and its prediction based on aerosol
577 hygroscopicity and composition in the Pearl Delta River (PRD) region during wintertime 2014, *Atmos.*
578 *Chem. Phys.*, 18, 16419-16437, doi:<https://doi.org/10.5194/acp-18-16419-2018>, 2018.

579 Crosbie, E., Youn, J. S., Balch, B., Wonaschutz, A., Shingler, T., Wang, Z., Conant, W. C., Betterton, E.
580 A., and Sorooshian, A.: On the competition among aerosol number, size and composition in predicting
581 CCN variability: a multi-annual field study in an urbanized desert, *Atmos Chem Phys*, 15, 6943-6958,
582 doi:<https://doi.org/10.5194/acp-15-6943-2015>, 2015.

583 Deng, Z. Z., Zhao, C. S., Ma, N., Ran, L., Zhou, G. Q., Lu, D. R., and Zhou, X. J.: An examination of
584 parameterizations for the CCN number concentration based on in situ measurements of aerosol activation
585 properties in the North China Plain, *Atmos. Chem. Phys.*, 13, 6227-6237,
586 doi:<https://doi.org/10.5194/acp-13-6227-2013>, 2013.

587 Dusek, U., Frank, G. P., Curtius, J., Drewnick, F., Schneider, J., Kürten, A., Rose, D., Andreae, M. O.,
588 Borrmann, S., and Pöschl, U.: Enhanced organic mass fraction and decreased hygroscopicity of cloud
589 condensation nuclei (CCN) during new particle formation events, *Geophys Res Lett*, 37,
590 doi:<https://doi.org/10.1029/2009GL040930>, 2010.

591 Dusek, U., Frank, G. P., Hildebrandt, L., Curtius, J., Schneider, J., Walter, S., Chand, D., Drewnick, F.,
592 Hings, S., Jung, D., Borrmann, S., and Andreae, M. O.: Size matters more than chemistry for cloud-
593 nucleating ability of aerosol particles, *Science*, 312, 1375-1378,
594 doi:<https://doi.org/10.1126/science.1125261>, 2006.

595 Fitzgerald, J. W.: Dependence of the Supersaturation Spectrum of CCN on Aerosol Size Distribution and
596 Composition, *J Atmos Sci*, 30, 628-634, doi:[https://doi.org/10.1175/1520-0469\(1973\)030](https://doi.org/10.1175/1520-0469(1973)030), 1973.

597 Fletcher, Squires, I. b. P., and Bowen, F. b. E. G.: *The Physics of Rainclouds*, 2011.



598 Frossard, A. A., Russell, L. M., Burrows, S. M., Elliott, S. M., Bates, T. S., and Quinn, P. K.: Sources and
599 composition of submicron organic mass in marine aerosol particles, *J Geophys Res-Atmos*, 119, 12977-
600 13003, doi:<https://doi.org/10.1002/2014jd021913>, 2014.

601 Geng, X. F., Zhong, G. C., Li, J., Cheng, Z. B., Mo, Y. Z., Mao, S. D., Su, T., Jiang, H. Y., Ni, K. W., and
602 Zhang, G.: Molecular marker study of aerosols in the northern South China Sea: Impact of atmospheric
603 outflow from the Indo-China Peninsula and South China, *Atmos Environ*, 206, 225-236,
604 doi:<https://doi.org/10.1016/j.atmosenv.2019.02.033>, 2019.

605 Gras, J. L.: CN, CCN and particle size in Southern Ocean air at Cape Grim, *Atmos Res*, 35, 233-251,
606 doi:[https://doi.org/10.1016/0169-8095\(94\)00021-5](https://doi.org/10.1016/0169-8095(94)00021-5), 1995.

607 Gras, J. L. and Keywood, M.: Cloud condensation nuclei over the Southern Ocean: wind dependence
608 and seasonal cycles, *Atmos. Chem. Phys.*, 17, 4419-4432, doi:<https://doi.org/10.5194/acp-17-4419-2017>,
609 2017.

610 Gysel, M., Crosier, J., Topping, D. O., Whitehead, J. D., Bower, K. N., Cubison, M. J., Williams, P. I.,
611 Flynn, M. J., McFiggans, G. B., and Coe, H.: Closure study between chemical composition and
612 hygroscopic growth of aerosol particles during TORCH2, *Atmos. Chem. Phys.*, 7, 6131-6144,
613 doi:<https://doi.org/10.5194/acp-7-6131-2007>, 2007.

614 H.R. Pruppacher, J. D. K.: *Microphysics of Clouds and Precipitation*, Atmospheric and Oceanographic
615 Sciences Library, Springer Dordrecht, XXII, 954 pp., <https://doi.org/10.1007/978-0-306-48100-0>, 2010.

616 Huang, S., Wu, Z., Wang, Y., Poulain, L., Höpner, F., Merkel, M., Herrmann, H., and Wiedensohler, A.:
617 Aerosol Hygroscopicity and its Link to Chemical Composition in a Remote Marine Environment Based
618 on Three Transatlantic Measurements, *Environ. Sci. Technol*, 56, 9613-9622,
619 doi:<https://doi.org/10.1021/acs.est.2c00785>, 2022.

620 Ipcc: Annex I: Observational Products [Trewin, B. (ed.)], in: *Climate Change 2021: The Physical Science*
621 *Basis. Contribution of Working Group I to the Sixth Assessment Report of the Intergovernmental Panel*
622 *on Climate Change*, edited by: Masson-Delmotte, V., Zhai, P., Pirani, A., Connors, S. L., Péan, C., Berger,
623 S., Caud, N., Chen, Y., Goldfarb, L., Gomis, M. I., Huang, M., Leitzell, K., Lonnoy, E., Matthews, J. B.
624 R., Maycock, T. K., Waterfield, T., Yelekçi, O., Yu, R., and Zhou, B., Cambridge University Press,
625 Cambridge, United Kingdom and New York, NY, USA, 2061–2086,
626 <https://doi.org/10.1017/9781009157896.015>, 2021.



627 Jayachandran, V., Safai, P. D., Soyam, P. S., Malap, N., Bankar, S. P., Varghese, M., and Prabha, T. V.:
628 Characterization of carbonaceous aerosols during the Indian summer monsoon over a rain-shadow region,
629 *Air Qual Atmos Hlth*, 15, 1713-1728, doi:<https://doi.org/10.1007/s11869-022-01211-1>, 2022.

630 Jimenez, J. L., Canagaratna, M. R., Donahue, N. M., Prevot, A. S., Zhang, Q., Kroll, J. H., DeCarlo, P.
631 F., Allan, J. D., Coe, H., Ng, N. L., Aiken, A. C., Docherty, K. S., Ulbrich, I. M., Grieshop, A. P., Robinson,
632 A. L., Duplissy, J., Smith, J. D., Wilson, K. R., Lanz, V. A., Hueglin, C., Sun, Y. L., Tian, J., Laaksonen,
633 A., Raatikainen, T., Rautiainen, J., Vaattovaara, P., Ehn, M., Kulmala, M., Tomlinson, J. M., Collins, D.
634 R., Cubison, M. J., Dunlea, E. J., Huffman, J. A., Onasch, T. B., Alfarra, M. R., Williams, P. I., Bower,
635 K., Kondo, Y., Schneider, J., Drewnick, F., Borrmann, S., Weimer, S., Demerjian, K., Salcedo, D., Cottrell,
636 L., Griffin, R., Takami, A., Miyoshi, T., Hatakeyama, S., Shimono, A., Sun, J. Y., Zhang, Y. M., Dzepina,
637 K., Kimmel, J. R., Sueper, D., Jayne, J. T., Herndon, S. C., Trimborn, A. M., Williams, L. R., Wood, E.
638 C., Middlebrook, A. M., Kolb, C. E., Baltensperger, U., and Worsnop, D. R.: Evolution of organic
639 aerosols in the atmosphere, *Science*, 326, 1525-1529, doi:<https://doi.org/10.1126/science.1180353>, 2009.

640 Kawana, K., Miyazaki, Y., Omori, Y., Tanimoto, H., Kagami, S., Suzuki, K., Yamashita, Y., Nishioka, J.,
641 Deng, Y. G., Yai, H., and Mochida, M.: Number-Size Distribution and CCN Activity of Atmospheric
642 Aerosols in the Western North Pacific During Spring Pre-Bloom Period: Influences of Terrestrial and
643 Marine Sources, *J Geophys Res-Atmos*, 127, e2022JD036690,
644 doi:<https://doi.org/10.1029/2022JD036690>, 2022.

645 Köhler, H.: The nucleus in and the growth of hygroscopic droplets, *Trans. Faraday Soc.*, 32, 1152-1161,
646 doi:<https://doi.org/10.1039/TF9363201152>, 1936.

647 Kuang, Y., Xu, W., Tao, J., Ma, N., Zhao, C., and Shao, M.: A Review on Laboratory Studies and Field
648 Measurements of Atmospheric Organic Aerosol Hygroscopicity and Its Parameterization Based on
649 Oxidation Levels, *Curr. Pollut. Rep*, 6, 410-424, doi:<https://doi.org/10.1007/s40726-020-00164-2>, 2020.

650 Lambe, A. T., Onasch, T. B., Massoli, P., Croasdale, D. R., Wright, J. P., Ahern, A. T., Williams, L. R.,
651 Worsnop, D. R., Brune, W. H., and Davidovits, P.: Laboratory studies of the chemical composition and
652 cloud condensation nuclei (CCN) activity of secondary organic aerosol (SOA) and oxidized primary
653 organic aerosol (OPOA), *Atmos. Chem. Phys.*, 11, 8913-8928, doi:[https://doi.org/10.5194/acp-11-8913-](https://doi.org/10.5194/acp-11-8913-2011)
654 2011, 2011.



- 655 Leena, P. P., Pandithurai, G., Anilkumar, V., Murugavel, P., Sonbawne, S. M., and Dani, K. K.: Seasonal
656 variability in aerosol, CCN and their relationship observed at a high altitude site in Western Ghats,
657 Meteorol Atmos Phys, 128, 143-153, doi:<https://doi.org/10.1007/s00703-015-0406-0>, 2016.
- 658 Liang, B., Cai, M., Sun, Q., Zhou, S., and Zhao, J.: Source apportionment of marine atmospheric aerosols
659 in northern South China Sea during summertime 2018, Environ. Pollut, 289, 117948,
660 doi:<https://doi.org/10.1016/j.envpol.2021.117948>, 2021.
- 661 Liu, P., Song, M., Zhao, T., Gunthe, S. S., Ham, S., He, Y., Qin, Y. M., Gong, Z., Amorim, J. C., Bertram,
662 A. K., and Martin, S. T.: Resolving the mechanisms of hygroscopic growth and cloud condensation nuclei
663 activity for organic particulate matter, Nat. Commun, 9, 4076, doi:<https://doi.org/10.1038/s41467-018-06622-2>, 2018.
- 665 Liu, S., Hu, M., Wu, Z., Wehner, B., Wiedensohler, A., and Cheng, Y.: Aerosol number size distribution
666 and new particle formation at a rural/coastal site in Pearl River Delta (PRD) of China, Atmos Environ,
667 42, 6275-6283, doi:<https://doi.org/https://doi.org/10.1016/j.atmosenv.2008.01.063>, 2008.
- 668 Liu, X. and Wang, J.: How important is organic aerosol hygroscopicity to aerosol indirect forcing?,
669 Environ. Res. Lett, 5, 044010, doi:<https://doi.org/10.1088/1748-9326/5/4/044010>, 2010.
- 670 Meng, J. W., Yeung, M. C., Li, Y. J., Lee, B. Y. L., and Chan, C. K.: Size-resolved cloud condensation
671 nuclei (CCN) activity and closure analysis at the HKUST Supersite in Hong Kong, Atmos. Chem. Phys.,
672 14, 10267-10282, doi:<https://doi.org/10.5194/acp-14-10267-2014>, 2014.
- 673 Moore, R. H., Nenes, A., and Medina, J.: Scanning Mobility CCN Analysis-A Method for Fast
674 Measurements of Size-Resolved CCN Distributions and Activation Kinetics, Aerosol Sci Tech, 44, 861-
675 871, doi:<https://doi.org/10.1080/02786826.2010.498715>, 2010.
- 676 Ou, H., Cai, M., Zhang, Y., Ni, X., Liang, B., Sun, Q., Mai, S., Sun, C., Zhou, S., Wang, H., Sun, j., and
677 Zhao, J.: Measurement Report: Seasonal variation and anthropogenic influence on cloud condensation
678 nuclei (CCN) activity in the South China Sea: Insights from shipborne observations during summer and
679 winter of 2021 [dataset], doi:<https://doi.org/10.6084/m9.figshare.25472545>, 2024.
- 680 Ovadnevaite, J., Zuend, A., Laaksonen, A., Sanchez, K. J., Roberts, G., Ceburnis, D., Decesari, S.,
681 Rinaldi, M., Hodas, N., Facchini, M. C., Seinfeld, J. H., and O' Dowd, C.: Surface tension prevails over
682 solute effect in organic-influenced cloud droplet activation, Nature, 546, 637-641,
683 doi:<https://doi.org/10.1038/nature22806>, 2017.



- 684 Petters, M. D. and Kreidenweis, S. M.: A single parameter representation of hygroscopic growth and
685 cloud condensation nucleus activity, *Atmos. Chem. Phys.*, 7, 1961-1971, doi:[https://doi.org/10.5194/acp-](https://doi.org/10.5194/acp-7-1961-2007)
686 [7-1961-2007](https://doi.org/10.5194/acp-7-1961-2007), 2007.
- 687 Pöhlker, M. L., Pöhlker, C., Ditas, F., Klimach, T., Hrabě de Angelis, I., Araújo, A., Brito, J., Carbone,
688 S., Cheng, Y., Chi, X., Ditz, R., Gunthe, S. S., Kesselmeier, J., Könemann, T., Lavrič, J. V., Martin, S. T.,
689 Mikhailov, E., Moran-Zuloaga, D., Rose, D., Saturno, J., Su, H., Thalman, R., Walter, D., Wang, J., Wolff,
690 S., Barbosa, H. M. J., Artaxo, P., Andreae, M. O., and Pöschl, U.: Long-term observations of cloud
691 condensation nuclei in the Amazon rain forest – Part 1: Aerosol size distribution, hygroscopicity, and
692 new model parametrizations for CCN prediction, *Atmos. Chem. Phys.*, 16, 15709-15740,
693 doi:<https://doi.org/10.5194/acp-16-15709-2016>, 2016.
- 694 Quinn, P. K., Bates, T. S., Coffman, D. J., and Covert, D. S.: Influence of particle size and chemistry on
695 the cloud nucleating properties of aerosols, *Atmos. Chem. Phys.*, 8, 1029-1042,
696 doi:<https://doi.org/10.5194/acp-8-1029-2008>, 2008.
- 697 Quinn, P. K., Bates, T. S., Coffman, D. J., Upchurch, L., Johnson, J. E., Moore, R., Ziemba, L., Bell, T.
698 G., Saltzman, E. S., Graff, J., and Behrenfeld, M. J.: Seasonal Variations in Western North Atlantic
699 Remote Marine Aerosol Properties, *J Geophys Res-Atmos*, 124, 14240-14261,
700 doi:<https://doi.org/10.1029/2019jd031740>, 2019.
- 701 Roldin, P., Ehn, M., Kurtén, T., Olenius, T., Rissanen, M. P., Sarnela, N., Elm, J., Rantala, P., Hao, L.,
702 Hyttinen, N., Heikkinen, L., Worsnop, D. R., Pichelstorfer, L., Xavier, C., Clusius, P., Öström, E., Petäjä,
703 T., Kulmala, M., Vehkamäki, H., Virtanen, A., Riipinen, I., and Boy, M.: The role of highly oxygenated
704 organic molecules in the Boreal aerosol-cloud-climate system, *Nat. Commun*, 10, 4370,
705 doi:<https://doi.org/10.1038/s41467-019-12338-8>, 2019.
- 706 Rose, D., Nowak, A., Achtert, P., Wiedensohler, A., Hu, M., Shao, M., Zhang, Y., Andreae, M. O., and
707 Pöschl, U.: Cloud condensation nuclei in polluted air and biomass burning smoke near the mega-city
708 Guangzhou, China - Part 1: Size-resolved measurements and implications for the modeling of aerosol
709 particle hygroscopicity and CCN activity, *Atmos. Chem. Phys.*, 10, 3365-3383,
710 doi:<https://doi.org/10.5194/acp-10-3365-2010>, 2010.
- 711 Ross, K. E., Piketh, S. J., Bruintjes, R. T., Burger, R. P., Swap, R. J., and Annegarn, H. J.: Spatial and
712 seasonal variations in CCN distribution and the aerosol-CCN relationship over southern Africa, *J*
713 *Geophys Res-Atmos*, 108, doi:<https://doi.org/10.1029/2002jd002384>, 2003.



714 Safai, P. D., Raju, M. P., Rao, P. S. P., and Pandithurai, G.: Characterization of carbonaceous aerosols
715 over the urban tropical location and a new approach to evaluate their climatic importance, *Atmos Environ*,
716 92, 493-500, doi:<https://doi.org/10.1016/j.atmosenv.2014.04.055>, 2014.

717 Savoie, D. L., Arimoto, R., Keene, W. C., Prospero, J. M., Duce, R. A., and Galloway, J. N.: Marine
718 biogenic and anthropogenic contributions to non-sea-salt sulfate in the marine boundary layer over the
719 North Atlantic Ocean, *J Geophys Res-Atmos*, 107, doi:<https://doi.org/10.1029/2001jd000970>, 2002.

720 Schmale, J., Henning, S., Decesari, S., Henzing, B., Keskinen, H., Sellegri, K., Ovadnevaite, J., Pohlker,
721 M. L., Brito, J., Bougiatioti, A., Kristensson, A., Kalivitis, N., Stavroulas, I., Carbone, S., Jefferson, A.,
722 Park, M., Schlag, P., Iwamoto, Y., Aalto, P., Aijala, M., Bukowiecki, N., Ehn, M., Frank, G., Frohlich, R.,
723 Frumau, A., Herrmann, E., Herrmann, H., Holzinger, R., Kos, G., Kulmala, M., Mihalopoulos, N., Nenes,
724 A., O'Dowd, C., Petaja, T., Picard, D., Pohlker, C., Poschl, U., Poulain, L., Prevot, A. S. H., Swietlicki,
725 E., Andreae, M. O., Artaxo, P., Wiedensohler, A., Ogren, J., Matsuki, A., Yum, S. S., Stratmann, F.,
726 Baltensperger, U., and Gysel, M.: Long-term cloud condensation nuclei number concentration, particle
727 number size distribution and chemical composition measurements at regionally representative
728 observatories, *Atmos. Chem. Phys.*, 18, 2853-2881, doi:<https://doi.org/10.5194/acp-18-2853-2018>, 2018.

729 Seinfeld, J. H. and Pandis, S. N.: *Atmospheric Chemistry and Physics: From Air Pollution to Climate*
730 *Change*, Wiley 2016.

731 Siegel, K., Neuberger, A., Karlsson, L., Zieger, P., Mattsson, F., Duplessis, P., Dada, L., Daellenbach, K.,
732 Schmale, J., Baccarini, A., Krejci, R., Svenningsson, B., Chang, R., Ekman, A. M. L., Riipinen, I., and
733 Mohr, C.: Using Novel Molecular-Level Chemical Composition Observations of High Arctic Organic
734 Aerosol for Predictions of Cloud Condensation Nuclei, *Environ. Sci. Technol*, 56, 13888-13899,
735 doi:<https://doi.org/10.1021/acs.est.2c02162>, 2022.

736 Sihto, S. L., Mikkila, J., Vanhanen, J., Ehn, M., Liao, L., Lehtipalo, K., Aalto, P. P., Duplissy, J., Petaja,
737 T., Kerminen, V. M., Boy, M., and Kulmala, M.: Seasonal variation of CCN concentrations and aerosol
738 activation properties in boreal forest, *Atmos. Chem. Phys.*, 11, 13269-13285,
739 doi:<https://doi.org/10.5194/acp-11-13269-2011>, 2011.

740 Sun, Q., Liang, B., Cai, M., Zhang, Y., Ou, H., Ni, X., Sun, X., Han, B., Deng, X., Zhou, S., and Zhao,
741 J.: Cruise observation of the marine atmosphere and ship emissions in South China Sea: Aerosol
742 composition, sources, and the aging process, *Environ. Pollut*, 316, 120539,
743 doi:<https://doi.org/10.1016/j.envpol.2022.120539>, 2023.



- 744 Tao, J., Kuang, Y., Ma, N., Hong, J., Sun, Y., Xu, W., Zhang, Y., He, Y., Luo, Q., Xie, L., Su, H., and
745 Cheng, Y.: Secondary aerosol formation alters CCN activity in the North China Plain, *Atmos. Chem.*
746 *Phys.*, 21, 7409-7427, doi:<https://doi.org/10.5194/acp-21-7409-2021>, 2021.
- 747 Topping, D. O., McFiggans, G. B., and Coe, H.: A curved multi-component aerosol hygroscopicity model
748 framework: Part 1 - Inorganic compounds, *Atmos. Chem. Phys.*, 5, 1205-1222,
749 doi:<https://doi.org/10.5194/acp-5-1205-2005>, 2005.
- 750 Tseng, Y. L., Yuan, C. S., Bagtasa, G., Chuang, H. L., and Li, T. C.: Inter-correlation of Chemical
751 Compositions, Transport Routes, and Source Apportionment Results of Atmospheric PM_{2.5} in Southern
752 Taiwan and the Northern Philippines, *Aerosol Air Qual Res*, 19, 2645-2661,
753 doi:<https://doi.org/10.4209/aaqr.2019.10.0526>, 2019.
- 754 Wang, Y., Chen, J., Wang, Q., Qin, Q., Ye, J., Han, Y., Li, L., Zhen, W., Zhi, Q., Zhang, Y., and Cao, J.:
755 Increased secondary aerosol contribution and possible processing on polluted winter days in China,
756 *Environ Int*, 127, 78-84, doi:<https://doi.org/10.1016/j.envint.2019.03.021>, 2019.
- 757 Wang, Y. Q.: MeteInfo: GIS software for meteorological data visualization and analysis, *Meteorol. Appl.*,
758 21, 360-368, doi:<https://doi.org/10.1002/met.1345>, 2014.
- 759 Weingartner, E., Burtscher, H., and Baltensperger, U.: Hygroscopic properties of carbon and diesel soot
760 particles, *Atmos Environ*, 31, 2311-2327, doi:[https://doi.org/10.1016/S1352-2310\(97\)00023-X](https://doi.org/10.1016/S1352-2310(97)00023-X), 1997.
- 761 Wu, C. and Yu, J. Z.: Determination of primary combustion source organic carbon-to-elemental carbon
762 (OC_{aEuro}-/aEuro-EC) ratio using ambient OC and EC measurements: secondary OC-EC correlation
763 minimization method, *Atmos. Chem. Phys.*, 16, 5453-5465, doi:[https://doi.org/10.5194/acp-16-5453-](https://doi.org/10.5194/acp-16-5453-2016)
764 2016, 2016.
- 765 Yang, M., Jalava, P., Wang, X.-F., Bloom, M. S., Leskinen, A., Hakkarainen, H., Roponen, M., Komppula,
766 M., Wu, Q.-Z., Xu, S.-L., Lin, L.-Z., Liu, R.-Q., Hu, L.-W., Yang, B.-Y., Zeng, X.-W., Yu, Y.-J., and Dong,
767 G.-H.: Winter and spring variation in sources, chemical components and toxicological responses of urban
768 air particulate matter samples in Guangzhou, China, *Sci. Total Environ*, 845, 157382,
769 doi:<https://doi.org/10.1016/j.scitotenv.2022.157382>, 2022.
- 770 Zhang, X. Y., Zhuang, G. S., Guo, J. H., Yin, K. D., and Zhang, P.: Characterization of aerosol over the
771 Northern South China Sea during two cruises in 2003, *Atmos Environ*, 41, 7821-7836,
772 doi:<https://doi.org/10.1016/j.atmosenv.2007.06.031>, 2007.



773 Zheng, G. J., Kuang, C. G., Uin, J., Watson, T., and Wang, J.: Large contribution of organics to
774 condensational growth and formation of cloud condensation nuclei (CCN) in the remote marine boundary
775 layer, *Atmos. Chem. Phys.*, 20, 12515-12525, doi:<https://doi.org/10.5194/acp-20-12515-2020>, 2020.
776



777 FIGURE CAPTION

778 Figure 1. The cruises of two shipborne observation.

779 Figure 2. Timeseries of (a) particle number size distribution, (b) mass concentration of NR-PM₁, and (c)
780 its fraction, (d) mass concentration of organic carbon and elemental carbon, (e) number concentration of
781 total particle and cloud condensation nuclei under the supersaturation of 0.1%, 0.2%, 0.4%, and 0.7%,
782 and (f) aerosol hygroscopicity. The number 1 means timeseries in summer and number 2 means it in
783 winter.

784 Figure 3. Particle number size distribution under effect of terrestrial air masses in summer (a) and winter
785 (b); Particle number size distribution under effect of mixed air masses in summer (c) and winter (d); The
786 red markers represent the activation diameters and hygroscopicity parameters corresponding to 0.1%,
787 0.2%, 0.4%, and 0.7% supersaturations in this study (without 0.1% in summer). The green markers
788 represent the hygroscopicity parameters reported in Atwood et al. (2017) for the southern South China
789 Sea during summer. The gray markers represent the hygroscopicity parameters documented in Cai et al.
790 (2018) for the Pearl River Delta region during winter.

791 Figure 4. The mass concentration of NR-PM₁, primary organic carbon, secondary carbon, elemental
792 carbon, and black carbon and their fraction under effect of different air masses in summer and winter.

793 Figure 5. Scatter plot of κ under the supersaturation of 0.2% and organic mass fraction with linear
794 regression.

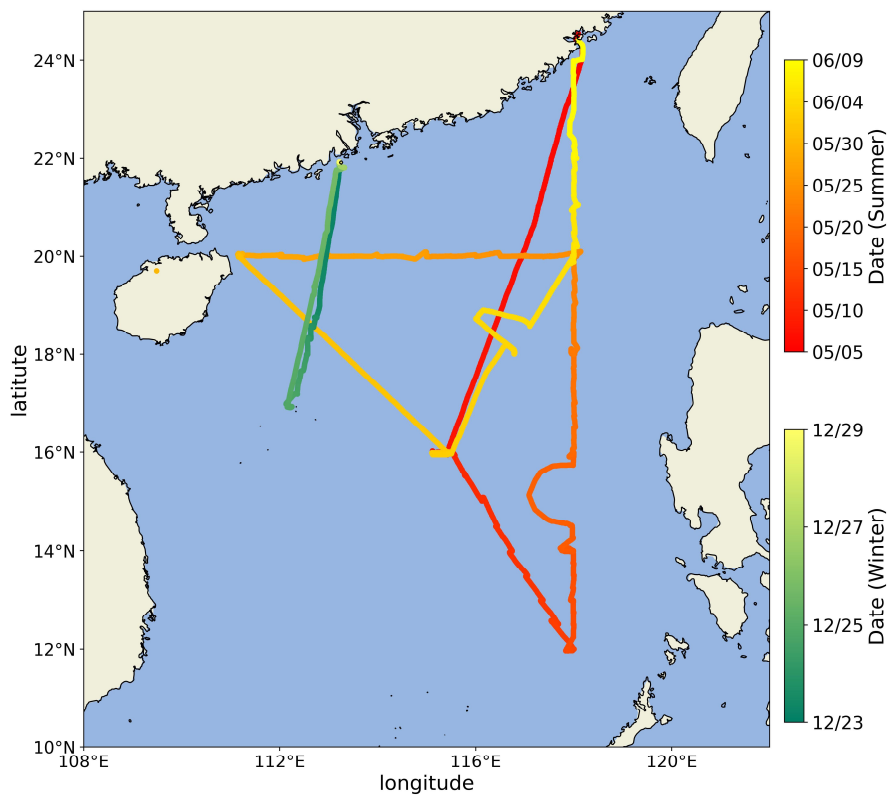
795 Figure 6. Activation ratio at supersaturation of 0.1%, 0.2%, 0.4%, and 0.7% under effect of terrestrial
796 and mixed air masses in summer and winter. The box extends from the first quartile (Q1) to the third
797 quartile (Q3) of the data, with a line at the median. The box extends from Q1 to Q3 of the data, with a
798 line at the median. The whiskers extend from the box by 1.5 times of the inter-quartile range (IQR). Flier
799 points are those passing the end of the whiskers.

800 Figure 7. Differences in activation fraction calculated from different particle size distributions and
801 activation diameters.

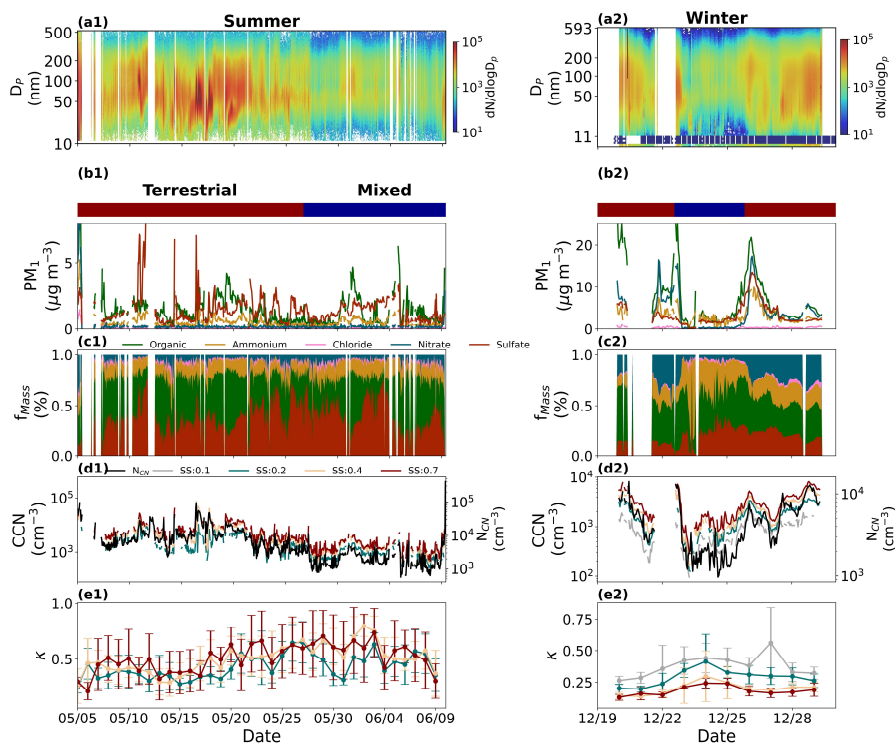
802 Figure 8. Variations of $\kappa_{SS:0.4\%}$, trace gases (NO_x and CO), OC/EC, BC, SOC/OC, mass fraction of
803 NR-PM₁ chemical composition, as well as number concentrations of nucleation mode, Aitken mode, and
804 accumulation mode with offshore distance under effect of terrestrial and mixed air masses in summer
805 and winter.



806 Figure 9. The difference between the calculated cloud condensation nuclei number concentration (NCCN)
807 using the D50 from the farthest and nearest offshore distances, along with the measured particle number
808 size distribution (PNSD), and the measured NCCN under the effect of terrestrial air masses in summer
809 (a1 and a2) and winter (c1 and c2); The difference between the calculated NCCN using the PNSD from
810 the farthest and nearest offshore distances, along with the measured D50, and the measured NCCN under
811 the effect of terrestrial air masses in summer (b1 and b2) and winter (d1 and d2). Δ NCCN refers to the
812 difference between calculated NCCN and observed NCCN, divided by the observed NCCN.
813
814



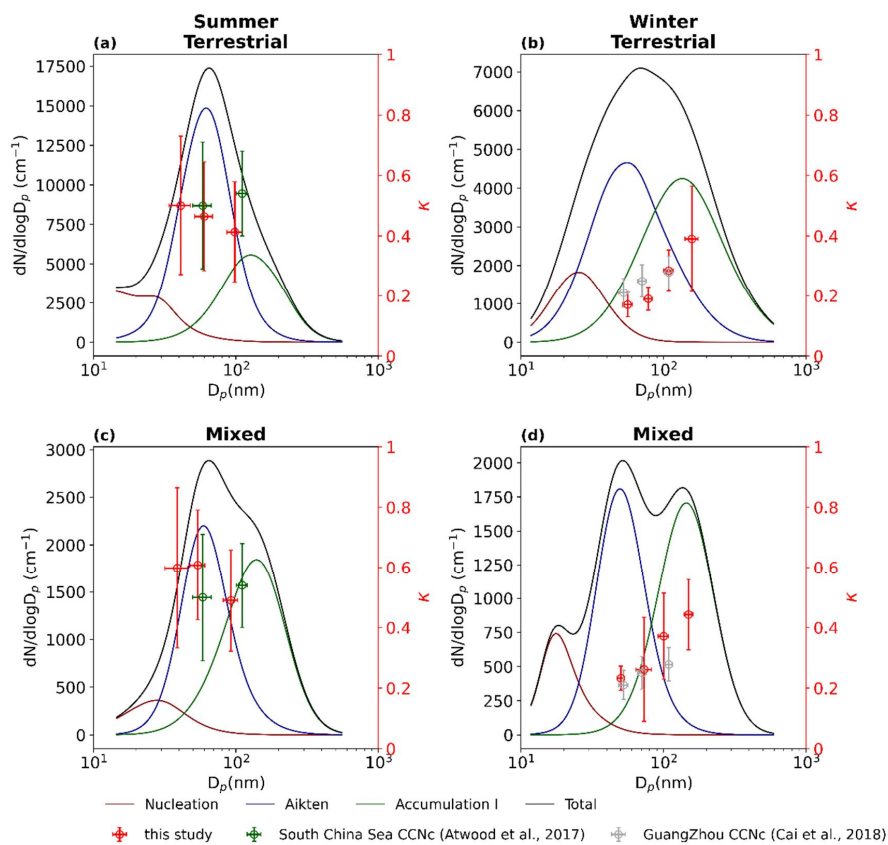
815
816 Fig. 1
817



818

819 Fig. 2

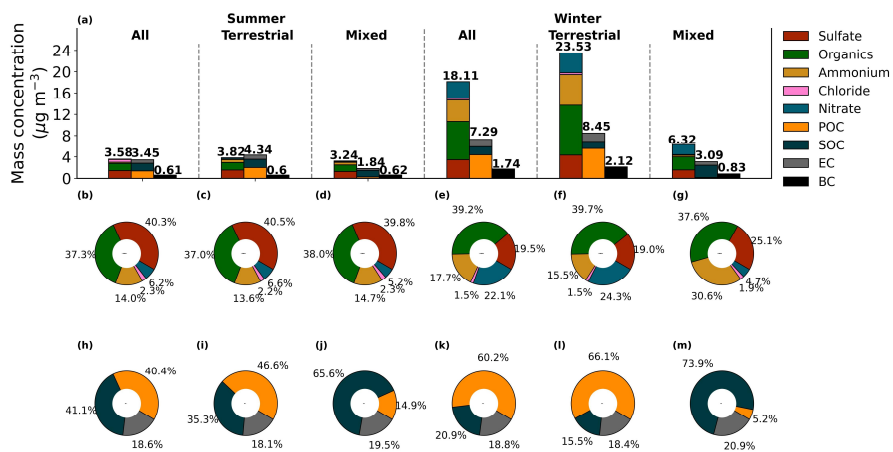
820



821

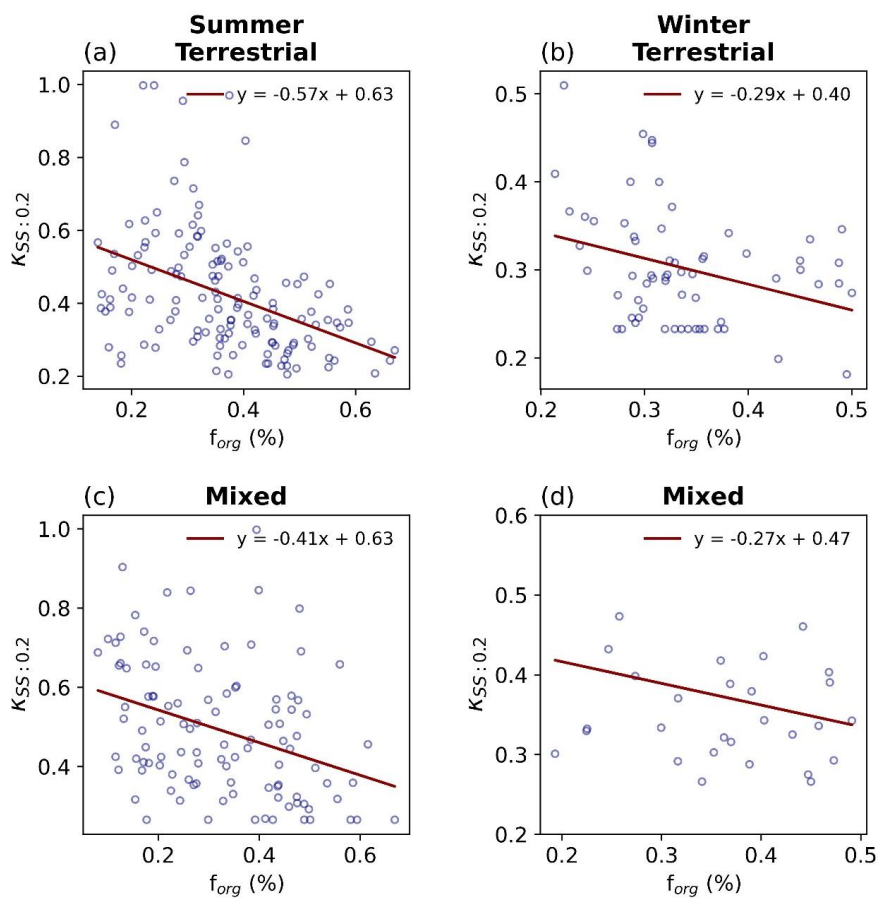
822 Fig. 3

823



824
825
826
827

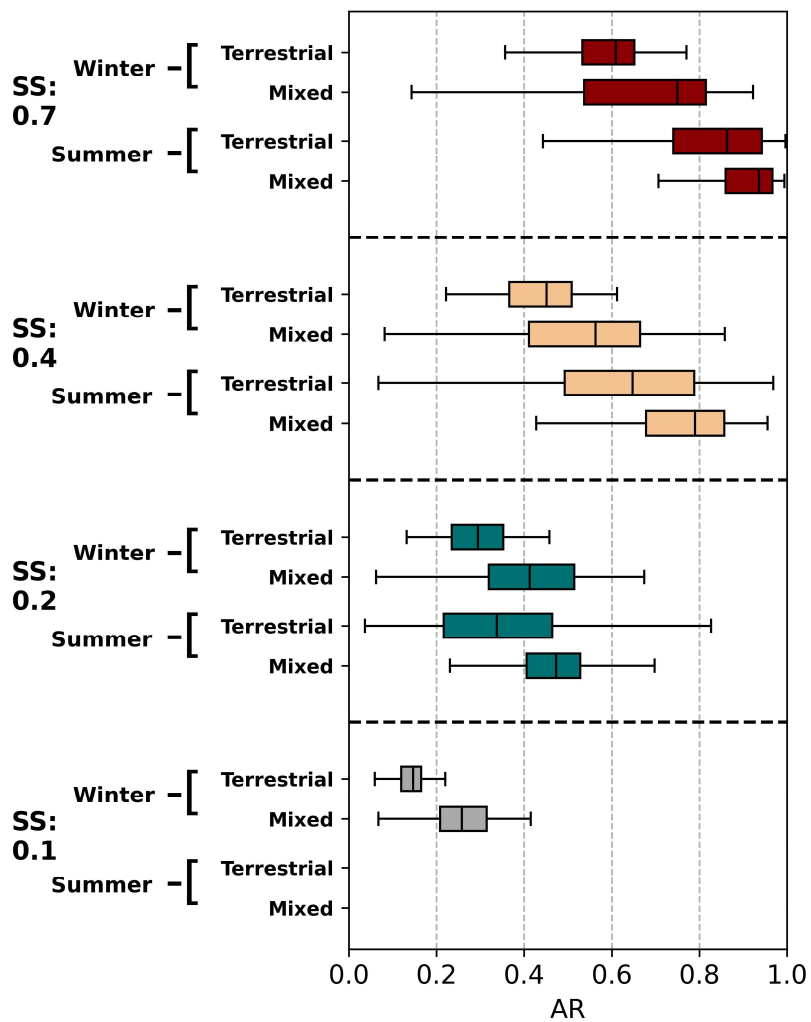
Fig. 4



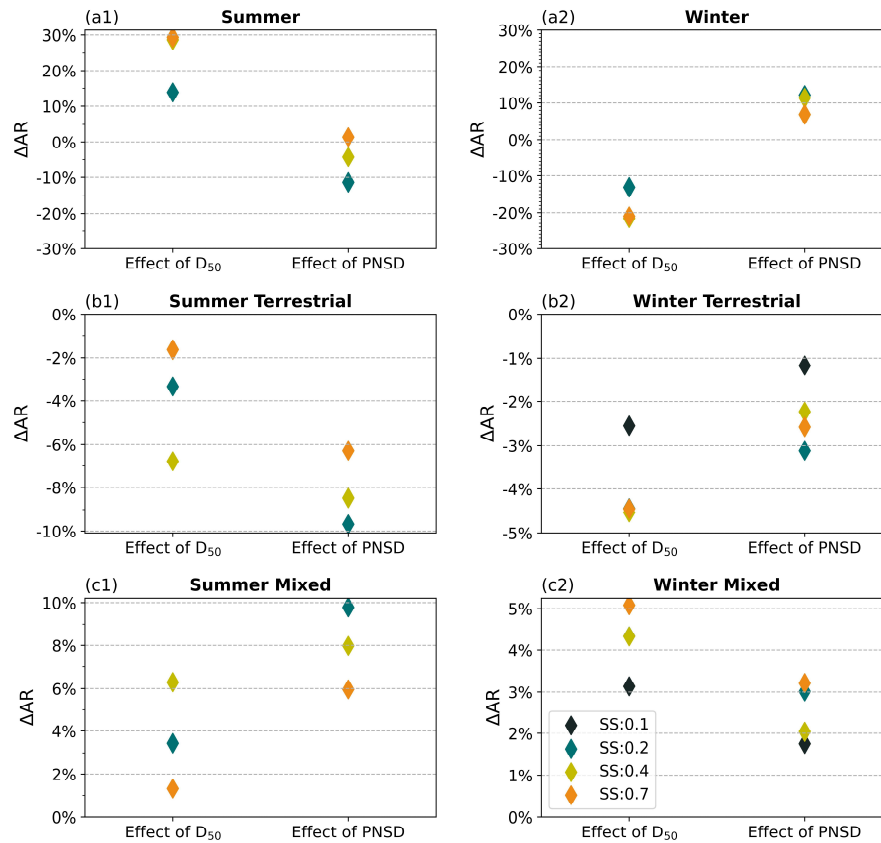
828

829 Fig.5

830



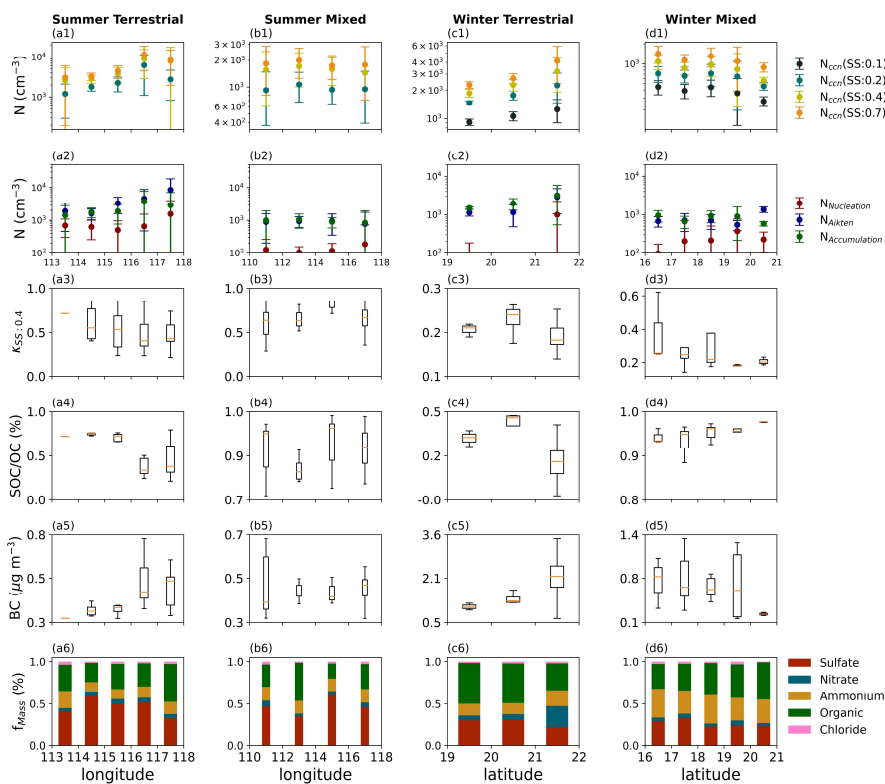
831
832 Fig. 6
833



834

835 Fig. 7

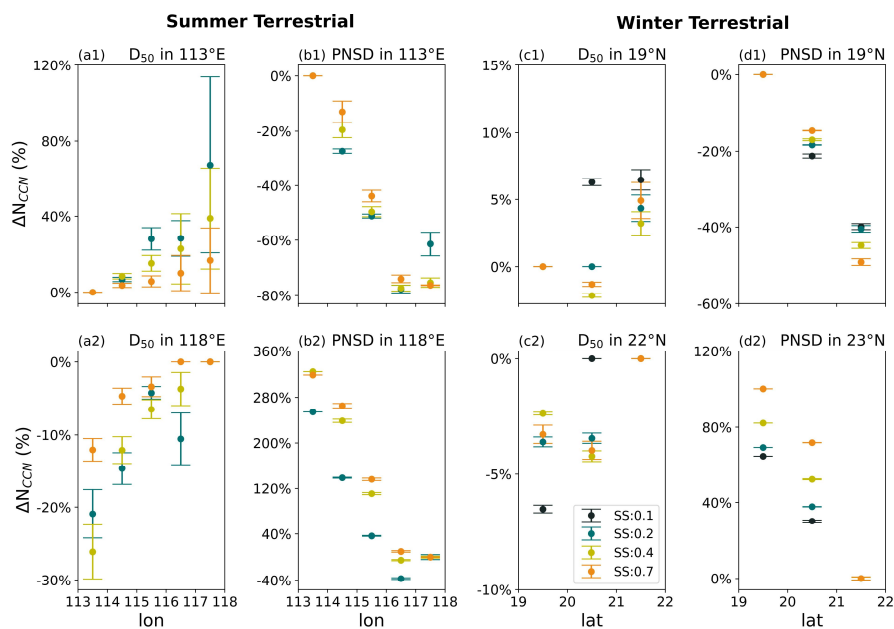
836



837

838 Fig. 8

839



840

841

842 Fig. 9

843

844